Localisation of Anatomical Soft Tissue Landmarks of the Head in CT Images

M. Ovinis, D. Kerr, K. Bouazza-Marouf, and M. Vloeberghs

Abstract—In this paper, algorithms for the automatic localisation of two anatomical soft tissue landmarks of the head, the medial canthus (inner corner of the eye) and the tragus (a small, pointed, cartilaginous flap of the ear), in CT images are described. These landmarks are to be used as a basis for an automated image-to-patient registration system we are developing. The landmarks are localised on a surface model extracted from CT images, based on surface curvature and a rule based system that incorporates prior knowledge of the landmark characteristics. The approach was tested on a dataset of near isotropic CT images of 95 patients. The position of the automatically localised landmarks was compared to the position of the manually localised landmarks. The average difference was 1.5 mm and 0.8 mm for the medial canthus and tragus, with a maximum difference of 4.5 mm and 2.6 mm respectively.The medial canthus and tragus can be automatically localised in CT images, with performance comparable to manual localisation.

Keywords—Anatomical soft tissue landmarks, automatic localisation, Computed Tomography (CT)

I. INTRODUCTION

IMAGE-TO-PATIENTregistration is a method where correspondence between 'image space' (an image of an anatomy) and 'patient space' (the anatomy itself) is established.Features to be co-registered that are used to facilitate the registration are known as a registration basis. Anatomical soft tissue landmarks of the head can be used as a basis for image to patient registration [1]–[2]. We have previously proposed [3]-[4] the use of the canthus and tragus as a registration basis for an automated, preoperative CT image to intraoperative patient registration system. The use of these landmarksavoids resorting to fiducial markers. At present, these landmarks are manually localised. If localised automatically, they could be used as a registration basis in an automated image-to-patient registration system. The localisation of these landmarks in patient space using close range photogrammetry has previously been reported by Gooroochurn et al [5]. In this paper, an approach to automatically localise the medial canthus and tragus in CT images is described.

The medial canthus (Fig. 1a) and tragus (Fig. 1b) are conventional soft tissue craniometric anatomical landmarks with the following definitions: The medial canthus is the inner corner of the eye where the upper and lower eyelids meet. The tragus is a small, pointed, cartilaginous flap in front of the external opening of the ear. As the tragus is a relatively large structure, the most lateral point of the tragus is chosen as the point which uniquely defines its position.

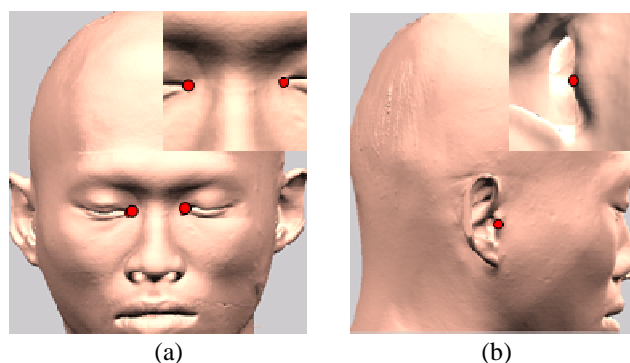
(a)   (b)

Fig. 1 (a) Medial canthus and (b) the most lateral point of the tragus

The majority of work on localising anatomical landmarks in head CT images is concerned with internal landmarks of the head e.g. tips of the frontal, temporal, and occipital horns of the ventricular system; saddle point of the zygomatic and nasal bone; and tip of the external occipital protuberance [6]-[8]. Early work on localising these anatomical landmarks in CT images used 3D generalisations of 2D differential operators/corner detectors [9]. A more recent approach used 3D deformable models [8],[10]. In this semi automatic approach, the user is required to provide a gross localisation of the landmarks, which the algorithm then refines, by fitting models of anatomical structures to their images. Recently, a method to automatically localised anatomical landmarks in CT images was proposed by Subburaj et al [11], who used surface curvature and prior knowledge of the gross spatial location of landmarks to localise anatomical landmarks of the knee-joint. However, their localisation technique, based on the relative location of landmarks, is not applicable in our work, as there are no other soft tissue landmarks that can be used to facilitate the localisation of the medial canthus and tragus.

M. Ovinis is a PhD scholar in the Department of Mechanical and Manufacturing Engineering, Loughborough University, LE11 3TU, Loughborough, UK (phone: +441509227579; fax: +441509227648; email: M.Ovinis2@lboro.ac.uk).

D. Kerr and K. Bouazza-Marouf are Senior Lecturers in the Department of Mechanical and Manufacturing Engineering, Loughborough University, LE11 3TU, Loughborough, UK (e-mail: d.kerr@lboro.ac.uk and k.bouazza-marouf@lboro.ac.uk respectively).

Prof. M. Vloeberghs is a Consultant Neurosurgeon at the Queen's Medical Centre, Nottingham University, NG7 2UH, Nottingham, UK (e-mail:Michael.Vloeberghs@Nottingham.ac.uk).

World Academy of Science, Engineering and Technology
International Journal of Biomedical and Biological Engineering
Vol:4, No:9, 2010

II. METHODOLOGY

The medial canthus and tragus is localised on a surface model of the head (the surface between the surrounding air and the voxels inside the head), extracted from CT images. As these landmarks exhibit characteristic surface curvature properties, a thresholded surface curvature map is used to localise these landmarks. However, the use of surface curvature alone is insufficient to localise these landmarks, as there will be many false detections. We use a rule-based system incorporating prior knowledge of the landmark characteristics to reduce the search space and avoid large localisation errors. Landmarksare identified based on having a geometric structure and spatial location consistent with the prior knowledge. A summary of the method is shown in flowchart form in Fig 2.
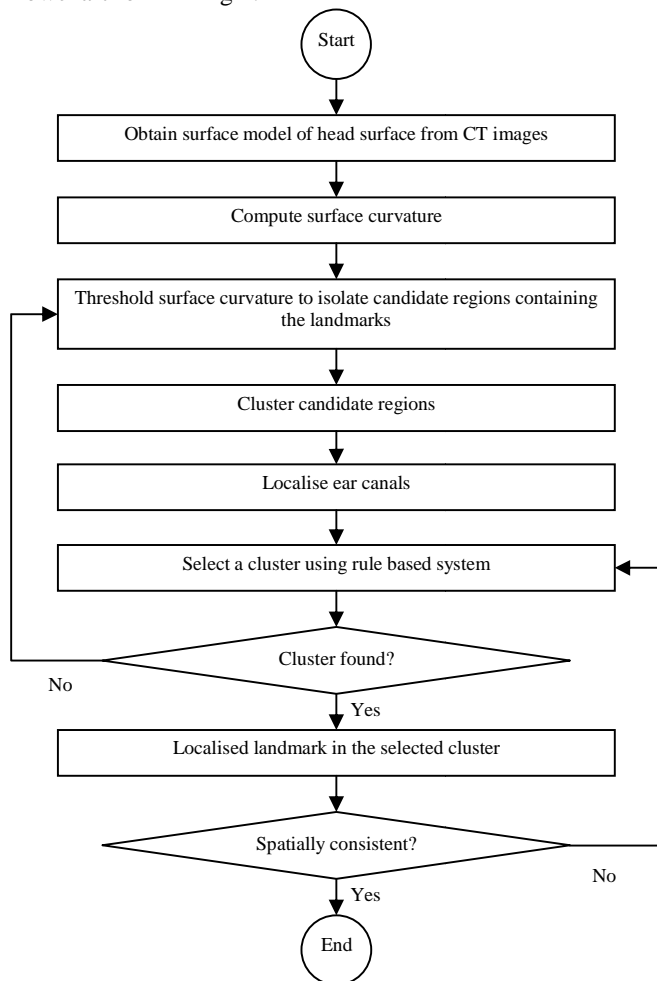

Fig. 2 Flowchart summarising the methodology

A. Landmark surface geometry

Characterising the geometry of the medial canthus and tragus is necessary in developing an algorithm to automatically localise these landmarks. Part of the difficulty in describing the geometry of anatomical landmarks in general is that their definitions are often fuzzy and are therefore difficult to translate into a formal mathematical description [13]. The medial canthus is the most medial point of a depressed region that forms a line which extends from the outer corner to the inner corner of the eye. This region exhibits high positive mean curvature and zero Gaussian curvature. The tragus is approximately semi-ellipsoid, and its most lateral point is the tip of this structure, a locally maximum point. It is characterised by negative mean curvature and high Gaussian curvature.

B. Curvature estimation

There are three approaches to calculate curvature of a surface represented by a mesh: fitting methods, discrete methods, and curvature tensor estimation [14]. In fitting methods, an analytic function, whose curvature can be computed, is fitted to a mesh locally. Fitting is computationally expensive. Discrete methods involve a direct estimation of the curvature at each vertex, by summing the curvature of each face or edge associated with the vertex. Discrete curvature methods are appealing because of their speed. However, they are sensitive to noise and mesh resolution. Curvature tensor estimation is similar to discrete methods, except that instead of estimating the curvature directly, the curvature tensor is estimated. Curvatures and principal directions are derived from the eigenvalues and eigenvectors of the curvature tensor.

Curvature tensor estimation is computationally less complex than fitting methods, although slightly slower than the discrete methods. They are elegant and free of unstable configurations, although certain vertex arrangements produces erroneous curvature estimates [15]. The curvature tensor estimation methodby Cohen-Steiner and Morvan [16] and Alliez et al. [17] is used in this work and is described next. For an arbitrary region, B, on a triangulated surface mesh, the curvature tensor, $\Im$, is the average of individual curvature tensors of edges, e, of the mesh over the region, as shown in Fig 3.

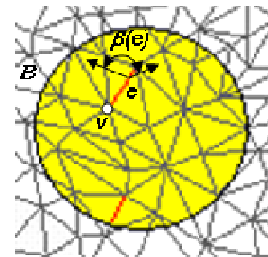

Fig. 3 Notations used in the curvature tensor estimation method

Formally, the curvature tensor, $\Im$, at an arbitrary vertex, v, on the mesh over an arbitrary region, B, is given by:

$$\Im(v) = \frac{1}{|B|} \sum_{edges\ e} \beta(e)|e \cap B|\bar{e}\ \bar{e}^t \qquad (1)$$

where $|B|$ is the surface area around the vertex $v$over which the curvature tensor $\Im$ is estimated, $\beta(e)$, is the signed angle between the normals of the two oriented triangles incident to edge e(positive if convex, negative if concave), $|e \cap B|$ is the length of $e \cap B$ (always between 0 and $|e|$), and $\bar{e}$is a unit vector in the same direction as e. A continuous tensor field

World Academy of Science, Engineering and Technology
International Journal of Biomedical and Biological Engineering
Vol:4, No:9, 2010

over the whole surface is obtained by linearly interpolating the piecewise curvature tensor at each vertex. The principal curvatures, κ_1 and κ_2, are the eigenvalues of the curvature tensor, $\Im$. The Gaussian and mean curvature can be computed from the principal curvature. The Gaussian curvature, K, is the product of the principal curvatures, κ_1 and κ_2:

$$K = \kappa_1 \kappa_2 \qquad (2)$$

The mean curvature, H, is the average of the principal curvatures, κ_1 and κ_2 :

$$H = \tfrac{1}{2}(\kappa_1 + \kappa_2) \qquad (3)$$

C. Surface model and curvature map

The following are the steps to generate a surface model and curvature map. First, the head region is segmented from CT images using intensity based thresholding. The threshold level is determined automatically using Otsu's method [18]. The segmented images contain holes in the region of interest and small, spurious regions in the background. To remove the holes, a morphological fill operation is applied. To remove the spurious regions, the largest connected binary component is selected. These operations are performed to eliminate additional structures of the extracted surface, which would complicate the automatic detection of the landmarks. The original image (Fig. 4a) is then multiplied with a mask consisting of the segmented image, and a grey level morphological fill operation is performed (Fig. 4b). Then, using a custom isosurface algorithm [19], a surface model of the head is extracted (Fig. 1).
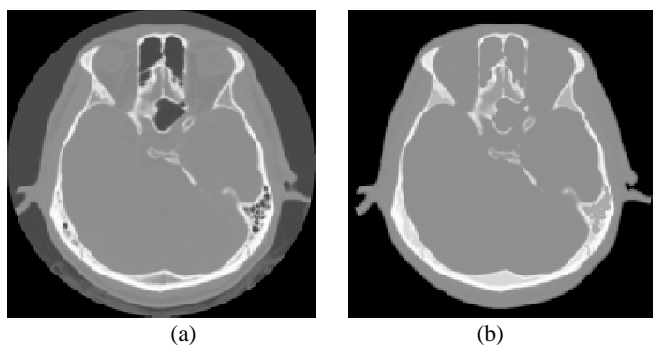

(a)　　　　　　　　(b)
Fig. 4 (a) Original and (b) segmented axial head CT image

A curvature map of the head surface model is generated using a curvature tensor estimation algorithm described in Section II. The curvature map for the eye region (Fig. 5a) and ear region (Fig. 5b) is illustrated in Fig. 5.
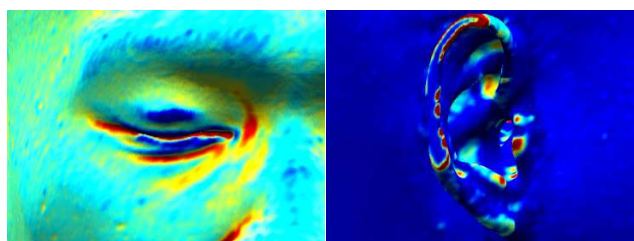

Fig. 5 (a) Curvature map of the eye and (b) ear

Curvature values have been normalised and colour coded for display purposes. Red and blue corresponds to areas of high and low curvature.

D. Clustering

The threshold surface curvature map contains many false regions i.e. regions other than those containing the landmarks (Fig. 6a). Clustering of the regions simplifies the analysis as multiple regions can be grouped and analysed using a divide and conquer approach (Fig. 6b).
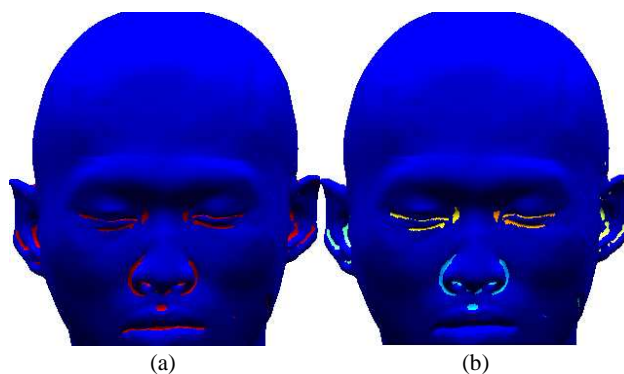

(a)　　　　　　　　(b)
Fig. 6 (a) Threshold surface curvature map (b) clustered regions

As the regions tend to be arbitrarily shaped, a density-based clustering algorithm, which works well with these types of regions, is used. In density based clustering, a cluster is formed if the density of its points exceeds a user defined threshold. The density-based spatial clustering of applications with noise (DBSCAN) algorithm [12] is used. DBSCAN formalises an intuitive notation of "clusters" and "noise" in a clustering application. The algorithm requires two only parameters: a distance measure, and the minimum number of points for a cluster to be formed.

E. Rule-based system

The selection of a cluster containing the landmarks is based on its spatial location and geometric structure. Spatially, the landmarks should exhibit bilateral symmetry. An allowable range of distance between the landmarks was used as a simple measure of bilateral symmetry. Geometrically, clusters containing the landmarks should have dimensions within a predefined range. Both the distance and allowable dimensions were determined empirically based on our dataset. If the localised landmarks are spatially or geometrically inconsistent, the entire process is repeated using a different cluster and/or a higher surface curvature threshold.

F. Localisation of the medial canthus

Regions of high positive mean curvature and zero Gaussian curvature correspond to candidate locations for the medial canthus. These regions are isolated by thresholding a curvature map of the surface using an empirically derived fixed threshold, and grouped using a density-based algorithm (Fig. 6). The clusters associated with the eye region are identified using nearest neigbour clustering based on the standard shape

World Academy of Science, Engineering and Technology
International Journal of Biomedical and Biological Engineering
Vol:4, No:9, 2010

and anatomy of the human face. The cluster with the maximum horizontal length in the eye region (Fig. 7b), with a horizontal length and vertical height within a predefinedrange,is selected as the most likely cluster containing the medial canthus.The medial canthus corresponds to the most medial point of this cluster. Once both the medial canthus are localised, bilateral symmetrybased on the separation distance between the medial canthi is assessed. If the symmetry condition is not met, the process is repeated using a different cluster and/or different mean curvature threshold. Fig. 7 illustrates the effect of varying the threshold level. Each colour corresponds to an individual cluster.
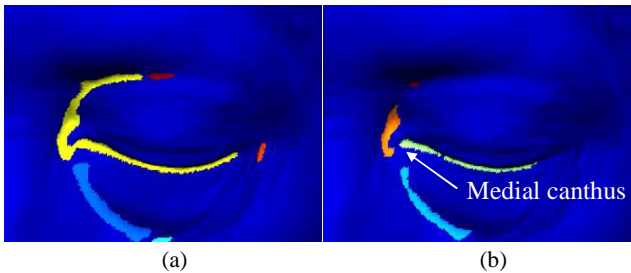

Fig. 7 Clusters corresponding (a) $C_{mean} \geq 0.01$ and $C_{gaussian} = 0$ (b) Cmean ≥ 0.015 and $C_{gaussian} = 0$.

In Fig. 7a, although the yellow clusterhas the maximum horizontal length,its vertical length is outside the allowable range. Increasing the threshold yields the cluster (green) containing the medial canthus (Fig. 7b).

Algorithm for the localisation of the medial canthus

Input: Vertices, V_i, of the triangular mesh surface model, the mean curvature, C_{mean}, and Gaussian curvature, $C_{gaussian}$
Algorithm:

1. Find candidate vertices, $v_j \in V_i$, {j=1,2,…,n} by thresholding based on mean surface curvature value, $C_{mean} \geq$ threshold and $C_{gaussian} = 0$ (Fig. 6a).

2. Group each vertex, v_j, into clusters, C_i, {i=1,2,….,p} using a density based clustering algorithm (Fig. 6b)

3. Group clusters, $c_j \in C_i$, {i=1,2} into two clusters, corresponding to the left and right eye region, using nearest neighbour clustering.

4. Select a cluster, $d_i \in c_j$ {$i = 1,2$} with maximum horizontal length with its horizontal length and vertical height within a predefinedrange (Fig. 7b)

5. Select most medial vertex, $v_{lmc} \in d_1$, for left medial canthus (Fig. 7b) and most medial vertex, $v_{rmc} \in d_2$, for right medial canthus.

6. Check the medial canthus for bilateral symmetry based on distance to the other medial canthus

7. Repeat steps 4 – 6 if step 6 fails, using a different cluster. If step 6 still fails, repeat steps 1 – 6 increasing the threshold.
Output: Vertices corresponding to the left and right medial canthus {v_{lmc}, v_{rmc}}.

G.Localisation of the tragus

Regions of high positive Gaussian curvature and negative mean curvature correspond to candidate locations for the tragus. Occasionally, the curvature map of the ear region contains many false regions because the outer edges of the ear are not always in the field of view and as such, the surface model of the ear region is not well defined (Fig 8).
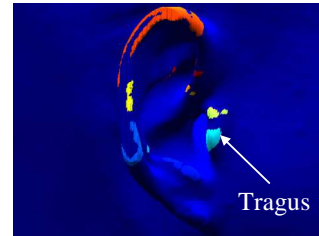

Fig. 8 Clusters in a thresholded surface curvature map of the ear.

It is therefore necessary to determine an estimate location of the cluster containing the tragus to avoid large positional errors. As the tragus is located close to the entrance of the ear canals and ear canals are prominent features in CT images (Fig. 9b, Fig. 9c),the location of the tragus is found by looking for the presence of ear canals in the CT axial and coronal planes and the outer ear structure in the CT sagittal plane (Fig. 11c).
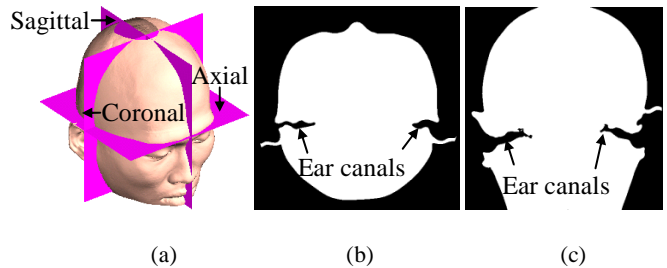

Fig.9 (a) Anatomical planes, (b) ear canals in CT axial plane (c) ear canals in CT coronal plane

A necessary step prior to the detection of the ear canals is to reorient the CT images using a rigid body transformation if the head orientation deviates by more than 15° from the forward facing position. The 2D orientation of the head is estimated as the angle between the horizontal axis and the major axis of an ellipse that has the same second-moments as the stacked axial head CT images (Fig. 10).
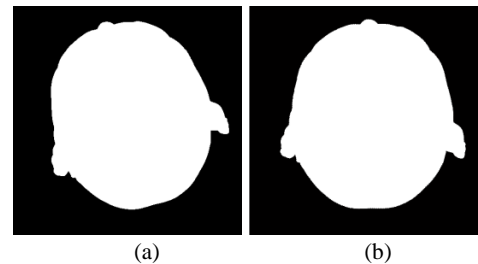

Fig. 10 (a) Deviation from forward facing position, and (b) reoriented head

The axial and coronal CT planes are then segmented and

World Academy of Science, Engineering and Technology
International Journal of Biomedical and Biological Engineering
Vol:4, No:9, 2010

skeletonised (Fig. 11). The axial and coronal planes whose skeleton endpoints are closest to the mid-sagittal plane correspond to the axial and coronal CT planes where the tragus is approximately located.
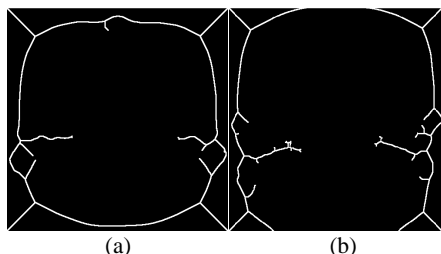

Fig. 11 Image skeleton for (a) Fig. 8(a) and (b) Fig. 8(b)

The sagittal plane where the tragus is approximately located may be found by scanning from the most lateral to the most medial sagittal plane (Fig. 12) until the Euler number of the largest connected binary region is equal to or is less than zero. In practice, morphological operations need to be performed to avoid false detections.
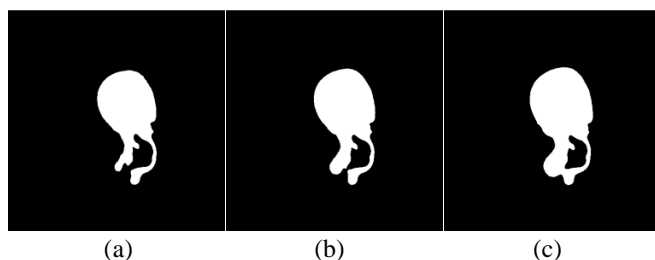

Fig. 12 Appearance of outer ear structure in CT sagittal view when scanned lateral to medial (left to right)

The largest region close to the estimated traggus positionis the most likely cluster containing the most lateral point of the tragus. The most lateral point of the tragus corresponds to a point with the highest Gaussian curvature in that cluster.

Algorithm for the localisation of the tragus

Input
1. Vertices, V_i, of the surface model triangular mesh,the mean curvature, C_{mean}, and Gaussian curvature, $C_{gaussian}$
Algorithm:
1. Reorient the head in the axial plane using a rigid transformation if the head orientation deviates more than 15° from the forward facing position (Fig. 10).
2. Estimate spatial location of the tragus. The corresponding axial and coronal planes are the axial and coronal plane with the longest ear canal, and the corresponding sagittal plane is the first sagittal plane (from lateral to medial), with a region whose Euler number is equal to, or less than, zero (Fig. 12c).
3. Find candidate vertices, $v_j \in V_i$ {j = 1,2,..,n} by thresholding based on $C_{gaussian} \geq 0.0001$ and $C_{mean} < 0$ (Fig. 8).
4. Group each vertex, v_j, into clusters, C_k, {$k = 1,2,….,p$} using density based clustering (Fig. 8)
5. Select largest cluster, c $\in C_k$, {$k = 1,2,….,p$}, within 10

mm from the estimated tragus location.
6. The vertices, v_{lt}, v_{rt}, $\in c$ with the highest Gaussian curvature value correspond to the most lateral point of the left and right tragus respectively.
Output: Vertices, {v_{rt}, v_{lt}}, corresponding to the most lateral point of the left and right tragus.

III. RESULTS AND DISCUSSION

A dataset consisting of near isotropic CT images of 95 patients acquired using a Toshiba Aquilion 16 CT scanner was used to test the algorithm. The images are 512 x 512 pixels with average in-slice pixel spacing and average slice thickness of 0.5 mm each, with no interslice spacing. The start and end scan location is from the skull vertex to at least the skull base, without any gantry tilt (gantry oriented parallel to the infraorbitomeatal line). The DICOM compliant CT images were transferred to a personal computer, and the landmarks were localised automatically.

A curvature map of the head surface model was obtained using the curvature tensor estimation method described in Section II. A neighbourhood B that approximates a disk around v with a radius equal to 1/100th of the diagonal of the bounding box containing the surface was used. To reduce the effect of noise, smoothing was applied to the mesh,although this has the effect of masking surface detail and blurred curvature estimates. The surface curvature map was thresholded using a$C_{mean} \geq 0.010$ and $C_{gaussian} = 0$to isolate candidate regions containing the medial canthus, and $C_{mean} < 0$ and $C_{gaussian} \geq 0.001$ to isolate candidate regions containing the most lateral point of the tragus. The DBSCAN method described in Section IIwas employed to cluster these regions. For the medial canthus, only clusters with a minimum size of 100 vertices (using a neighbourhood radius of 5 mm) were considered. Clusters with less than 100 vertices are abandoned as it is most likely noise. The algorithms described in Section II were used to select candidate clusters containing the medial canthus and the tragus. Estimates of the tragus location (Fig. 13) were found to be always within 10 mm of its actual location.
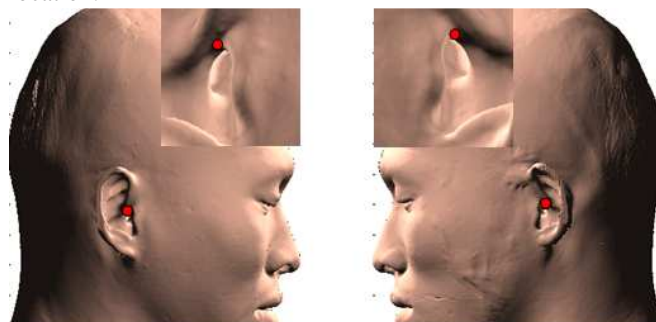

Fig. 13 Estimated tragus position

To check the bilateral symmetry of the left and right medial canthus, a separation distance of 15 - 40 mm, 30 mm and 20 mm in the sagittal, coronal and axial planes was used. For the left and right tragus, a separation distance of 100 - 200 mm, 40 mm and 40 mm was used. The relatively large separation

World Academy of Science, Engineering and Technology
International Journal of Biomedical and Biological Engineering
Vol:4, No:9, 2010

distance used for the coronal and axial planes is to account for head tilt, which is present in some of the images in the dataset. Because of the large separation distances used, the bilateral symmetry check is useful to prevent large localisations errors only. Fig. 14 illustrates the automatically localised medial canthus (Fig. 14a) and most lateral point of the tragus (Fig. 14b).
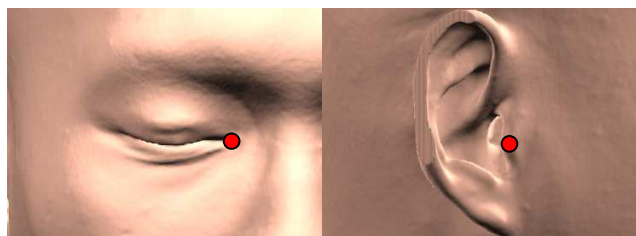

Fig. 14 The automatically localised (a) medial canthus and (b) most lateral point of the tragus

The difference between the locations of the landmarks found manually and automatically using the proposed method is expressed as the root mean square Euclidean distance between the two. Manual localisation was based on the perceived landmark location,the accuracy of which depends on the examiners experience and perception. The mean difference for the medial cantus is 1.5 mm, with a maximum difference of 4.5 mm. The mean difference for the tragus is 0.8 mm with a maximum difference of 2.6 mm.

Although no anatomical ground truth exists, it can be argued that automatic localisation of the most lateral point of the tragus, and to a lesser extent the medial canthus, is more accurate than manual localisation. This is because determining the exact location of the landmarks based on visual inspection is difficult. However, for the medial canthus, there are isolated cases where automatic localisation can produce large localisation errors. This is because the shape of the cluster and the corresponding perceived location of the medial canthus vary greatly depending on the threshold level (Fig. 15).
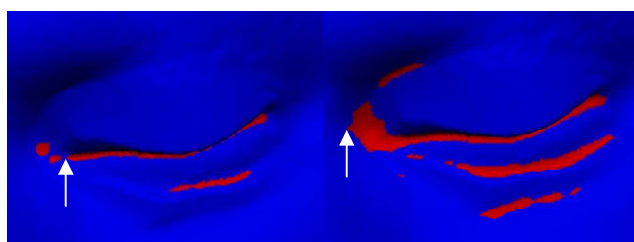

Fig. 15 Perceived location of the medial canthus at different thresholds, (a) $C_{mean} \geq 0.025$ and $C_{gaussian} = 0$ (b) $C_{mean} \geq 0.01$ and $C_{gaussian} = 0$

In this work, a fixed threshold (which is incremented if no cluster that satisfies the rule is found) is used. A threshold based on an arbitrary upper limit of a curvature histogram was considered but the presence of outliers due to imperfect segmentation greatly affects the resulting threshold value. For the majority of the images, the cluster containing the medial canthus is usually robust to the threshold level.

As we are developing this technique for three neurosurgical procedures normally performed without image-guidance i.e. using a freehand technique, the difference in localisation using a manual and automated technique is acceptable and is within our required 5 mm clinical accuracy [3, 4]. Images of four patients were excluded from the analysis as the medial canthus was not well defined in their CT images. Future work involves refining the algorithm to perform cluster analysis e.g. cluster shape, to prevent localisation errors such as those illustrates in Fig. 15.

IV. Conclusion

A methodology to automatically localise the medial canthus and tragus in CT images was presented. The basic approach was to exploit the surface curvature properties of the medial canthus and tragus. A rule system based on prior knowledge of the landmark geometric structure and spatial location was used to facilitate localisation, as surface curvature properties alone results in many false detections. The medial canthus and tragus can be localised on CT images, with performance comparable to manual localisation, based on the approach presented.

References

[1] P. A. Woerdeman, P. W. Willems, H. J. Noordmans, C. A. Tulleken and J. W. van der Sprenkel, "Application accuracy in frameless image-guided neurosurgery: A comparison study of three patient-to-image registration methods," J. Neurosurg., vol. 106, pp. 1012-1016, Jun, 2007.

[2] S. Wolfsberger, K. Rossler, R. Regatschnig and K. Ungersbock, "Anatomical landmarks for image registration in frameless stereotactic neuronavigation," Neurosurg. Rev., vol. 25, pp. 68-72, Mar, 2002.

[3] M. Gooroochurn, M. Ovinis, D. Kerr, K. Bouazza-Marouf and M. Vloeberghs, "A Registration Framework for Preoperative CT to Intraoperative White Light Images," Proc. Medical Image Understanding and Analysis, pp. 184-188, 2009.

[4] M. Gooroochurn, D. Kerr, K. Bouazza-Marouf; M.Ovinis, " Facial recognition techniques applied to the automated registration of patients in the emergency treatment of head injuries," Proceedings of the Institution of Mechanical Engineers, Part H: Journal of Engineering in Medicine (in press).

[5] M. Gooroochurn, D. Kerr, K. Bouazza-Marouf and M. Vloeberghs, "Extraction of Craniofacial Landmarks for Preoperative to Intraoperative Registration," in Sixth International Conference on Signal and Image Processing, .

[6] S. Frantz, K. Rohr and H. S. Stiehl, "Localization of 3D Anatomical Point Landmarks in 3D Tomographic Images Using Deformable Models," Lecture Notes In Computer Science, pp. 492-501, 2000.

[7] S. Frantz, K. Rohr and H. S. Stiehl, "Development and validation of a multi-step approach to improved detection of 3D point landmarks in tomographic images," Image Vision Comput., vol. 23, pp. 956-971, 2005.

[8] S. Wörz and K. Rohr, "Localization of anatomical point landmarks in 3D medical images by fitting 3D parametric intensity models," Med. Image Anal., vol. 10, pp. 41-58, 2006.

[9] K. Rohr, H. Stiehl, R. Sprengel, W. Beil, T. Buzug, J. Weese and M. Kuhn, "Point-based elastic registration of medical image data using approximating thin-plate splines," in Visualization in Biomedical Computing, 1996, pp. 297-306.

[10] M. Alker, S. Frantz, K. Rohr and H. Siegfried Stiehl, "Improving the robustness in extracting 3D point landmarks from 3D medical images using parametric deformable models," in Medical Image Computing and Computer-Assisted Intervention–MICCAI 2001, 2001, pp. 582-590.

[11] K. Subburaj, B. Ravi and M. Agarwal, "Automated identification of anatomical landmarks on 3D bone models reconstructed from CT scan images," Comput. Med. Imaging Graphics, vol. 33, pp. 359-368, 2009.

[12] M. Ester, H. P. Kriegel, J. Sander and X. Xu, "A density-based algorithm for discovering clusters in large spatial databases with noise," in Proc. 2nd Int. Conf. on Knowledge Discovery and Data Mining, Portland, OR, AAAI Press, 1996, pp. 226-231.

[13] P. Li, B. D. Corner and S. Paquette, "Automatic landmark extraction from three-dimensional head scan data," in Proceedings of SPIE, 2002, pp. 169.

[14] T. D. Gatzke and C. M. Grimm, "Estimating curvature on triangular meshes," Int. J. Shape Model., vol. 12, pp. 1, 2006.

[15] S. Rusinkiewicz, "Estimating curvatures and their derivatives on triangle meshes," in 3D Data Processing, Visualization and Transmission, 2004. 3DPVT 2004. Proceedings. 2nd International Symposium on, 2004, pp. 486-493.

[16] D. Cohen-Steiner and J. M. Morvan, "Restricted delaunay triangulations and normal cycle," in Proceedings of the Nineteenth Annual Symposium on Computational Geometry, 2003, pp. 312-321.

[17] P. Alliez, D. Cohen-Steiner, O. Devillers, B. Lévy and M. Desbrun, "Anisotropic polygonal remeshing," 2003.

[18] N. Otsu, "A threshold selection method from gray-level histograms," Automatica, vol. 11, pp. 285-296, 1975.

[19] The MathWorks, Source Code for the Matlab Isosurface Function. 2007.